frontiers in Neurology

ORIGINAL RESEARCH
published: 11 November 2021
doi: 10.3389/fneur.2021.745770

Neurovascular Reactivity in the Aging Mouse Brain Assessed by Laser Speckle Contrast Imaging and 2-Photon Microscopy: Quantification by an Investigator-Independent Analysis Tool

Fatma Burcu Seker[1]*, *Ziyu Fan*[1], *Benno Gesierich*[1], *Malo Gaubert*[1], *Rebecca Isabella Sienel*[1] and *Nikolaus Plesnila*[1,2]*

[1] Institute for Stroke and Dementia Research, Munich University Hospital and University of Munich, Munich, Germany, [2] Munich Cluster for Systems Neurology (SyNergy), Munich, Germany

OPEN ACCESS

Edited by:
Dong Ming,
Tianjin University, China

Reviewed by:
Hirac Gurden,
Université de Paris, France
Hongyang Lu,
Medtronic Inc, Ireland

***Correspondence:**
Fatma Burcu Seker
burcu.seker@med.uni-muenchen.de
Nikolaus Plesnila
nikolaus.plesnila@
med.uni-muenchen.de

Specialty section:
This article was submitted to Applied Neuroimaging, a section of the journal Frontiers in Neurology

Received: 22 July 2021
Accepted: 08 October 2021
Published: 11 November 2021

Citation:
Seker FB, Fan Z, Gesierich B, Gaubert M, Sienel RI and Plesnila N (2021) Neurovascular Reactivity in the Aging Mouse Brain Assessed by Laser Speckle Contrast Imaging and 2-Photon Microscopy: Quantification by an Investigator-Independent Analysis Tool. Front. Neurol. 12:745770. doi: 10.3389/fneur.2021.745770

The brain has a high energy demand but little to no energy stores. Therefore, proper brain function relies on the delivery of glucose and oxygen by the cerebral vasculature. The regulation of cerebral blood flow (CBF) occurs at the level of the cerebral capillaries and is driven by a fast and efficient crosstalk between neurons and vessels, a process termed neurovascular coupling (NVC). Experimentally NVC is mainly triggered by sensory stimulation and assessed by measuring either CBF by laser Doppler fluxmetry, laser speckle contrast imaging (LSCI), intrinsic optical imaging, BOLD fMRI, near infrared spectroscopy (NIRS) or functional ultrasound imaging (fUS). Since these techniques have relatively low spatial resolution, diameters of cerebral vessels are mainly assessed by 2-photon microscopy (2-PM). Results of studies on NVC rely on stable animal physiology, high-quality data acquisition, and unbiased data analysis, criteria, which are not easy to achieve. In the current study, we assessed NVC using two different imaging modalities, i.e., LSCI and 2-PM, and analyzed our data using an investigator-independent Matlab-based analysis tool, after manually defining the area of analysis in LSCI and vessels to measure in 2-PM. By investigating NVC in 6–8 weeks, 1-, and 2-year-old mice, we found that NVC was maximal in 1-year old mice and was significantly reduced in aged mice. These findings suggest that NVC is differently affected during the aging process. Most interestingly, specifically pial arterioles, seem to be distinctly affected by the aging. The main finding of our study is that the automated analysis tool works very efficiently in terms of time and accuracy. In fact, the tool reduces the analysis time of one animal from approximately 23 h to about 2 s while basically making no mistakes. In summary, we developed an experimental workflow, which allows us to reliably measure NVC with high spatial and temporal resolution in young and aged mice and to analyze these data in an investigator-independent manner.

Keywords: neurovascular coupling, hypercapnia, laser speckle contrast imaging, two-photon microscopy, aging, investigator-independent analysis

INTRODUCTION

Since the brain stores very little energy, proper neuronal function depends on a constant supply of glucose and oxygen via cerebral blood flow. During increased neuronal activity, the need for nutrients increases and the necessary excess energy is delivered via a tightly regulated redistribution of blood flow to these active areas by dilation of cerebral blood vessels. This regulation of cerebral blood flow (CBF) by the crosstalk between neurons and cerebral vessels is called "neurovascular coupling" or NVC (1, 2). NVC responses can be utilized as an indicator of neuronal activity. Under pathological conditions, NVC may be used to detect dysfunctions of the cerebrovascular system (3–5).

To investigate NVC *in vivo*, three different steps are needed: (1) a stimulation paradigm, (2) a fast technique to measure CBF or to visualize cerebral vessel reactivity, and (3) an unbiased and reliable method for data analysis. The first step depends on which region of the brain is studied. Typically, odor and visual cues, electrical or tactile sensory stimulations of the whiskers or the paws are used (6–9). The second prerequisite can be achieved using non-invasive optical methods based on the speckle pattern of moving red blood cells (Laser Speckle Contrast Imaging, LSCI). LSCI is a very powerful imaging tool for the 2-D visualization of perfusion dynamics in tissues (10–12). Another imaging method for visualizing the dynamics of the cerebral vasculature is two-photon microscopy (2-PM) (13–15). 2-PM is a state-of-the-art confocal scanning microscopy technique with a high spatial and temporal resolution able to visualize pial vessels, penetrating arterioles, and deep cortical microvessels *in vivo*. The final, but equally critical step is data analysis. The software provided with commercially available LSCI units has mainly been developed for data acquisition in single human subjects and has therefore only limited analysis capabilities. This is particularly true when it comes to the analysis of data sets acquired at different time points and in whole groups of subjects. Therefore, commercially available LSCI analysis solutions are not entirely suitable for research purposes. Also analyzing images obtained by 2-PM is a time-consuming manual process prone to investigator bias. Therefore, the main aim of the current study is to present a novel tool for the analysis of LSCI and 2-PM data to establish a flexible, software-based analysis pipeline for an automated and investigator-independent analysis of the obtained data sets.

To test our new experimental workflow, we used a model of physiological aging, a paradigm well-known to be associated with an age-related decrease in NVC. The world population is aging and over 30% of the people in western countries will be older than 65 years of age by 2050 (16). Aging causes significant structural changes in brain volume, in the dendritic arbor, spine and synapse numbers, and vasculature (17, 18). Among this population, cognitive impairments related to vascular changes are responsible for at least 20% of all dementia cases (19). Surely, NVC as a key homeostatic regulator is inevitably affected by these vascular changes (20). Sensory-evoked NVC responses are indirect measures of neuronal activation and any alteration in NVC can predict underlying pathology (21, 22). A substantial number of publications from various laboratories suggests impaired NVC in aged humans and experimental animals (23–27). It has been shown that age strongly alters CBF regulation in humans, specifically steady-state CBF decreases progressively during the aging process concomitant with an increase in CBF pulsatility after midlife (28). Also, structurally, cerebrovascular pathologies involving small arteries and arterioles are very common in the aged brain (29–31). Therefore a deep understanding of how NVC changes during aging is an important prerequisite in order to decipher the mechanisms underlying cerebrovascular disease, dementia, and neurodegeneration (32–34). Aging affects the normal structure and function of the neurovascular unit (NVU). Aged mice show decreased astrocyte end-feet density, reduced pericyte coverage in the hippocampus, more activated microglia, and reduced CBF as compared to young mice (35). Moreover, aging and concomitant metabolic disorders such as obesity impair NVC in animals and humans thereby making the aging brain more vulnerable to age-related neurodegenerative disorders such as Alzheimer's and Parkinson's Disease (4, 36, 37). Therefore, deciphering how NVC is affected by aging may lead to new therapeutic strategies for these disorders.

MATERIALS AND METHODS

Experimental Animals

All experimental procedures were conducted according to institutional guidelines of the University of Munich and were approved by the Government of Upper Bavaria (animal protocol number: Vet_2-15-196). In all parts of the experiments, 6–8 weeks old C57BL/6N mice were purchased from Charles River Laboratories (Sulzfeld, Germany). Mice at the age of 6–8 weeks were categorized as young and mice at the age of 1 year and 2 years were categorized as aged. The mice were aged in the animal facility of the Institute of Stroke and Dementia Research. All mice were housed in groups of five in isolated ventilated HEPA filtered cages with a 12-h light/dark cycle with *ad libitum* access to food and water. All cages had standard enrichment.

Chronic Cranial Window Implantation

A chronic cranial window was implanted over the left somatosensory cortex between the coronal and the sagittal suture. The rostromedial corner of the window was placed as close as possible to Bregma. Mice received buprenorphine (0.1 mg/kg) 30 min before surgery for analgesia and anesthesia was induced with 5% isoflurane and maintained with 2% isoflurane in 70% room air and 30% O_2 during surgery. A feedback-controlled heating pad was used to maintain body temperature at 37°C. Animals were fixed in a stereotactic frame using a nose clamp and the scalp was incised along the midline. Lidocaine (2%) was applied topically onto the skull as a local anesthetic and a round craniotomy with a diameter of 4 mm was performed above the somatosensory cortex and covered with a glass window. A plastic ring (diameter: 1 cm; weight: 0.1 g) was glued on top of the cranial window to form a water reservoir. After surgery, mice were placed in a pre-heated wake-up box (32°C) until all vital functions recovered. All mice received buprenorphine

and enrofloxacin (10 mg/kg s.c.) once daily for three days after surgery .

Whisker Stimulation

Three weeks after window implantation, mice received medetomidine (0.05 mg/kg, sc) for light sedation. After 10 min animals were anesthetized with 2% isoflurane and placed in a stereotactic frame. Afterwards, isoflurane was gradually reduced to 0.5–0.75% (in 70/30% Air/O_2) and whisker stimulation was performed over one minute by manually or mechanically stroking the contralateral (right) vibrissae with a brush at a frequency of 1–2 Hz. For 2-PM we developed a custom made motorized brush holder and use the same stimulation protocol as for the manual stimulation. The procedure was repeated three times with two min intervals (**Figure 1A**).

CO_2 Challenge

To evoke hypercapnic hyperemia, mice were ventilated with 10% CO_2 and 30% O_2 in room air for five min (**Figure 2A**). End-tidal CO_2 was measured in % with a capnograph (**Figure 2A**, right) and recorded using a digital data acquisition system (PowerLab, AD Instruments, Australia).

Measurement and Analysis of Local Cerebral Blood Flow by Laser Speckle Imaging

A laser speckle contrast imager (LSCI, Perimed, Järfälla, Sweden) was positioned 10.4 cm above the chronic cranial window and a 0.5 x 0.5 mm field of the cortex was imaged at 4.4 Hz. The data was recorded using the software supplied with the device (Pimsoft, Perimed, Järfälla, Sweden) and analyzed using a custom Matlab script (MATLAB, R2016b, The MathWorks, Natick, MA). First, a spherical region around the rim of the cranial window containing the exposed cortex (ROI), was drawn manually. For each pixel within the ROI, the perfusion signal was filtered with a cut-off frequency of 0.004 Hz to remove any signal drift and allows re-alignment of the acquired frames. This process is important while the brain and cerebral vessels move slightly due to heart beat and breathing. Hence, when using high resolution imaging, e.g., LSCI or 2-PM, images acquired at different time points shift slightly. Therefore, re-alignment is necessary to correctly allocate measurements obtained over time to exactly the same pixel. This filter was implemented using the MATLAB functions cheby1 and filtfilt to design a Chebyshev Type I filter of order 2 and to perform zero-phase digital filtering. Then a threshold was defined using Otsu's method, to detect stimulation periods automatically. The correct detection of stimulation periods was verified visually. To account for a potentially ramp-like increase of the perfusion signal at the beginning of the stimulation, the perfusion signal was averaged within 10 and 30 s after the automatically detected stimulation onset and normalized to the baseline perfusion signal, defined individually for each stimulation period as the average signal within 40 to 10 s before the automatically detected stimulation onset. The hereby resulting, normalized response of the perfusion signal to the stimulation was then averaged across stimulation periods. First individually for each animal and then across animals within each experimental group. To allow averaging across animals, the images, cropped around the spherical ROI, were resized to an image matrix of 120 x 120 pixels. For a better understanding of the individual responses, heat maps were also acquired for individual animals (**Figure 1B**).

Measurement and Analysis of Vessel Diameter by *in vivo* Two-Photon Microscopy

Two-photon microscopy (2-PM) was performed the day after the LSCI imaging using the same anesthesia protocol as described above. For visualizing the cerebral vasculature 0.1 ml of fluorescein isothiocyanate (2,000 kDa) was injected through the tail vein using a mouse tail illuminator (Braintree Scientific, USA). Then mice were transferred under the 2-PM. Pial and parenchymal vessels in the region of the barrel cortex were visualized as time series videos (2 s per frame) at a depth of 50–100 µm with a 10x Zeiss EC Plan—NeoFluar objective using a Li: Ti laser tuned to 800 nm. The whisker stimulation protocol was followed by 5 min 10% CO_2 challenge. A custom-made automated brush holder was used for whisker stimulation while imaging with 2-PM (**Figure 3A**). For this device, a small brush and a voltage controller for frequency adjustments were mounted to a 300 rpm (6 V) battery-powered motor (Walfront, China). A gooseneck holder was used to fix the motor on the imaging platform, which allowed fine-tuning the angle of the brush.

Vessel diameter analysis was performed using a custom-made Matlab routine (MathWorks version R2020a, Natick, Massachusetts, USA; www.mathworks.com) based on imshow3D developed by Maysam Shahedi (https://www.mathworks.com/matlabcentral/fileexchange/41334-imshow3d) and on a Zeiss LSM file reader developed by Cy Y (Zeiss Laser Scanning Confocal Microscope LSM file reader; https://github.com/joe-of-all-trades/lsmread). First, all images have been inspected and the ones containing artifacts (heavy motion between frames, low signal-to-noise ratio) were removed. Then, time series videos were binarized, and diameter and percent change graphs were displayed. Then, line segments were drawn by the user between the vessel walls. Every time a line was drawn, the diameter of the vessel in µm along time frames were calculated by counting the number of voxels with a value of 1 ("1" corresponds to a vessel, while "0" to the background) intersecting with the drawn line and multiplied by the voxel size. Of note, some erythrocytes passing through the vessel are reducing the intensities of specific voxels, which could lead to underestimation of vessel diameter. To minimize this effect, the thickness of the line was defined to 4 voxels and the computation of vessel diameter was thus adapted by averaging the lines around the drawn line. Based on the computation of vessel diameters along time, output graphs are displayed and updated for each new line and depicted with the same color as the line drawn on the image (**Figure 3A**, lower left). Moreover, automatic detection of percentage peak change was provided thanks to the Matlab routine. This peak detection was based on three parameters defined in the graphical interface. Briefly, the algorithm first computed the baseline diameter by averaging a predefined number of initial frames (no stimulation).

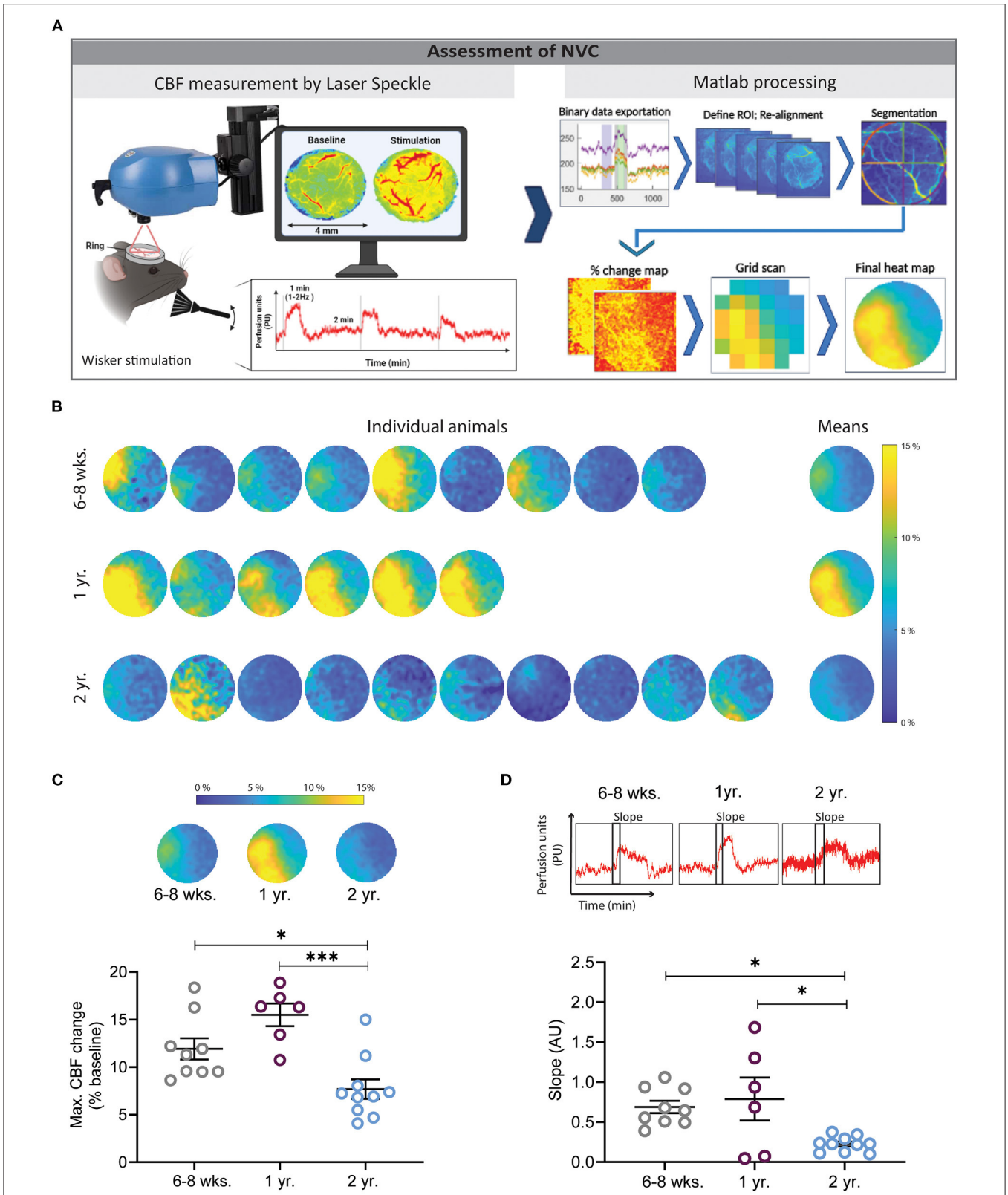

FIGURE 1 | Assessment of neurovascular coupling (NVC) using laser speckle contrast imaging (LSCI) and a Matlab-based analysis pipeline. **(A)** Experimental setup for whisker stimulation and data analysis. Data visualization with LSCI shows a flow map and a perfusion trace (left), data processing steps show binary data exportation, *(Continued)*

FIGURE 1 | ROI alignment, segmentation, % change map, grid preparation for quantification, and final averaged heat map (right). **(B)** Heat maps of cerebral perfusion (CBF) in individual mice of different ages following whisker stimulation. Each perfusion map was created by averaging LSCI values from three whisker stimulations. Mean depicts the average of all animals in one group. The dark blue color indicates no or small changes in cortical perfusion, while the yellow color indicates increases of cortical perfusion of up to 15%. **(C)** Quantification of maximal CBF changes. Young and 1-year-old mice had significantly higher NVC responses in comparison to 2 years old mice (*$P < 0.05$: 6–8 weeks vs. 2 years old, ***$P < 0.001$: 1 year vs. 2 year, One-way ANOVA). **(D)** Quantification of the velocity of CBF increase after whisker stimulation by slope analysis. Two year old mice had a significantly slower CBF increase in comparison to young and 1 year old mice (*$P < 0.05$: 6–8 weeks vs. 2 year and 1 year vs. 2 year) (n = 6–10 mice/group, mean ± SEM, One-way ANOVA).

For the peak detection, the difference between the subsequent frames (with stimulation), and the baseline was calculated. After the end of a peak, a new baseline was computed, and the peak detection continued in the subsequent frames. The detected peaks were then displayed in the first graph, in the same color as the line drawn on the image (see screenshots, **Figure 3A**, lower right). The slope of dilation between the maximal vessel diameter of a detected peak and related baseline was also calculated automatically using the following formula:

$$\text{Slope} = \frac{diameter_{max} - diameter_{baseline}}{time_{max} - time_{baseline}}$$

with $diameter_{\max}$, $time_{\max}$, the diameter of the maximal value in the peak and the peak time, and $diameter_{baseline}$, $time_{baseline}$, baseline diameter and the time on when this baseline was calculated (last timepoint before the detection of the peak). This slope was then normalized by the baseline vessel diameter. Finally, the percent of change was calculated by the Matlab routine as the difference between the maximal vessel diameter of a detected peak and related baseline as:

$$\text{Percent change} = \frac{diameter_{max} - diameter_{baseline}}{diameter_{baseline}} \times 100$$

and displayed. For each drawn segment, all vessel diameters along time and information on peaks (start, end, slope, percentage of change) have also been exported in a table for subsequent statistical analyses.

Data Availability

Scripts will be shared upon request.

Statistics

Statistical analyses were performed with GraphPad Prism 7.0 software (GraphPad Software, San Diego, California USA). First, data were tested for normal distribution. Student t-test was used to compare two sets of normally distributed data. Multiple groups were compared with one-way ANOVA or one-way ANOVA on ranks depending on the presence or absence of normal distribution or two-way ANOVA for repetitive measurements. Differences with $P < 0.05$ were considered statistically significant.

RESULTS

In this study, we developed a fast, reliable, and unbiased data processing tool for the analysis of neurovascular reactivity (NVC and CO_2 inhalation) assessed by LSCI and 2-PM. While LSCI provides information about CBF changes in the superficial layers of the cerebral cortex, *in vivo* 2-PM imaging directly visualizes diameter changes of individual cerebral vessels. For the validation of our newly developed analysis tools, we used aging as a model.

Decreased Neurovascular Coupling in Aged Mice

Mice were given three subsequent whisker stimulations (**Figure 1A**). All LSCI data were first acquired with Pimsoft software®. After the acquisition, data were extracted in binary format (.dat) and processed with a custom-made Matlab tool. The results were exported to a spreadsheet file and further analyzed and plotted. Furthermore, the Matlab tool generated an averaged image of all three stimulations, created CBF heat maps of individual mice, and allowed to average CBF values of all investigated mice in one single heat map (**Figure 1B**). The heat maps show an increased CBF in the area of the somatosensory cortex whereas CBF remained unchanged in the unstimulated surrounding cortex. CBF values from the heat maps could be extracted as numerical data and plotted. Two year-old mice had a 46 and 59% lower CBF response as compared to young and 1-year-old mice, respectively (**Figure 1C**, *$P < 0.05$: young vs. 2 year old, ***$P < 0.001$: 1 year vs. 2 year). No significant difference was found between young and 1-year-old mice. Moreover, 1-year-old mice had a moderately higher NVC response in comparison to young mice (**Figure 1C**). The slope of the CBF peak after the NVC stimulation was analyzed and a reduced slope was found in 2-years-old mice in comparison to young and 1-year-old mice, respectively (**Figure 1D**, *$P <$ 0.05: young vs. 2 year and 1 year vs. 2 years), indicating a slower response in this age group. No difference was found between young and 1-year-old mice (**Figure 2D**).

Decreased and Sluggish CO_2 Reactivity in Aged Mice

Following whisker stimulation, animals received 10% CO_2 by inhalation to induce hypercapnia and subsequent cerebral hyperemia. End tidal pCO_2 was assessed by microcapnometry and CBF was measured by LSCI (**Figure 2A**). A typical CBF response consists of an increase in CBF within one min after CO_2 inhalation followed by a plateau phase and a gradual recovery phase after termination of CO_2 inhalation (**Figure 2B**). Two-year-old mice showed a slower and lower CO_2 response curve in comparison to young and 1-year-old mice [$F_{(280,\ 2380)} = 2.329$, ***$P < 0.0001$, 2-way ANOVA]. The peak response in 2-year-old mice was reduced by 31 and 25% in comparison to young and 1-year-old mice, respectively (**Figure 2C**, *$P < 0.05$: young vs. 2 year). Not only the degree, but also the velocity of the

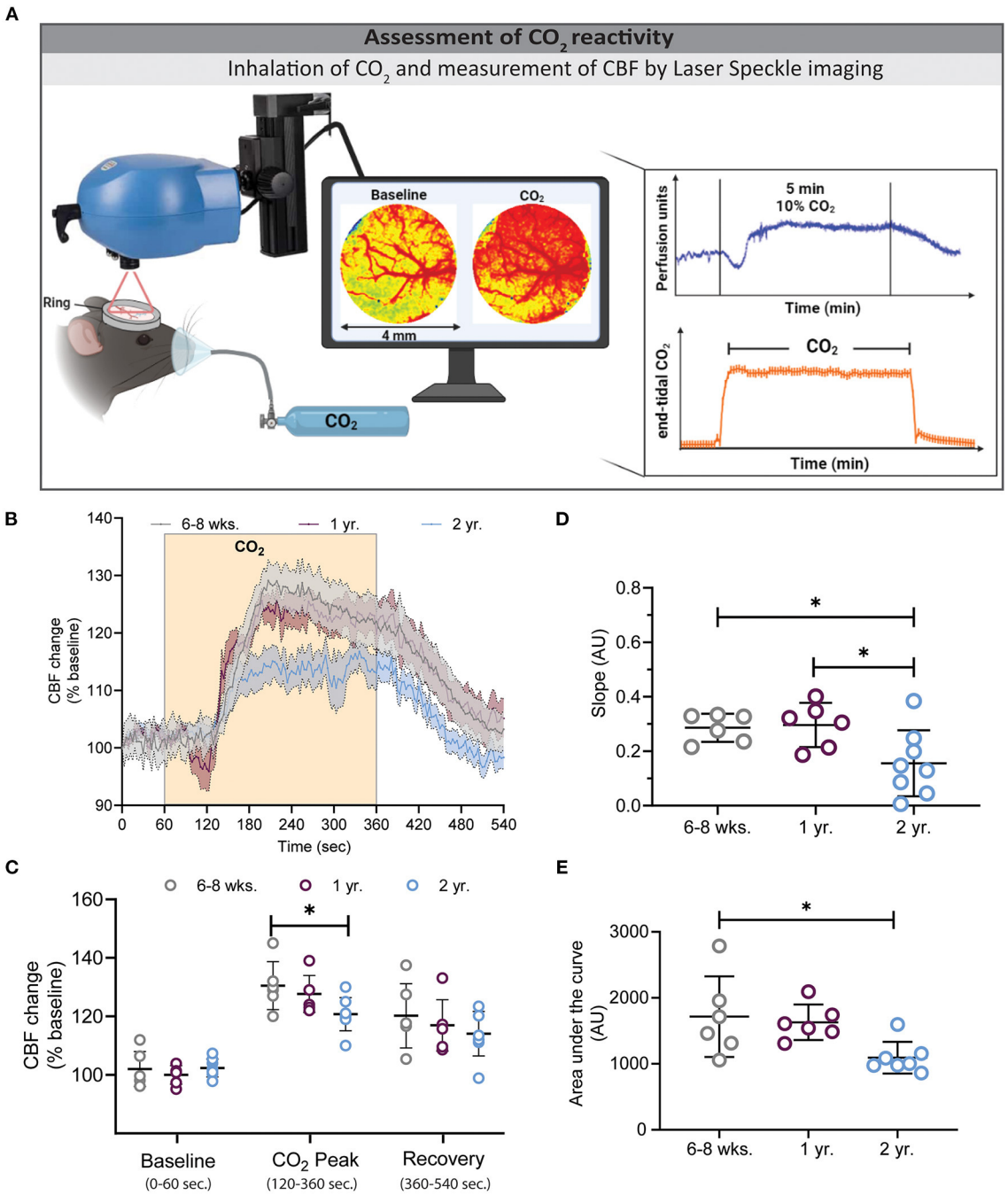

FIGURE 2 | Assessment of CO_2 reactivity using laser speckle contrast imaging (LSCI). **(A)** Experimental setup of the CO_2 challenge (left) and exemplary traces for LSCI perfusion (top right) and end-tidal CO_2 (bottom right). **(B)** CBF changes before, during, and after hypercapnia in the three investigated age groups. Two-year-old mice showed a low **(C)** and slow **(D)** CBF increase during hypercapnia, whereas young and 1-year-old mice had higher peak values (*$P < 0.05$: 6–8 weeks vs. 2 year), and faster slope changes (*$P < 0.05$: 6–8 weeks vs. 2 year and 1 year vs. 2 year). **(E)** Quantification of the area under the curve (AUC) of graph B depicts smaller AUC in 2 year old mice in comparison to 6–8 weeks and 1 year old mice (*$P < 0.05$) (mean ± SEM, $n = 6$–8 mice/group, One-way ANOVA).

CBF response was reduced in 2-year-old mice as indicated by a reduced slope of the CBF increase (**Figure 2D**, *$P < 0.05$: young vs. 2 year and 1 year vs. 2 year). As an integrative measure of the whole CBF response after hypercapnia we calculated the area under the curve (AUC). As expected from the previous measurements, also this value was significantly reduced in 2-year-old mice (**Figure 2E**, *$P < 0.05$: young vs. 2 year and 1 year vs. 2 year).

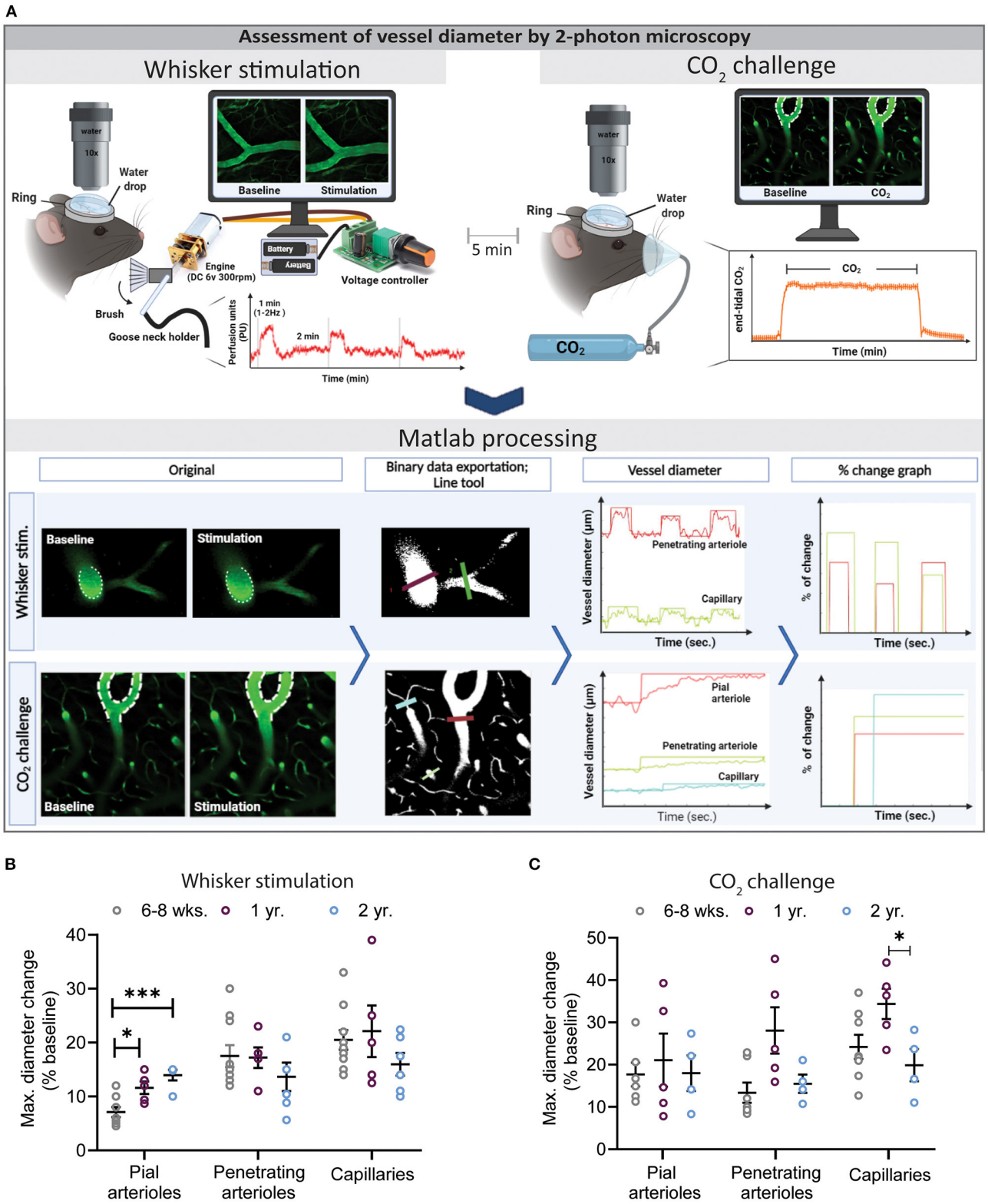

FIGURE 3 | Assessment of vessel diameter by 2-photon microscopy. **(A)** Experimental setup for whisker stimulation (top left) and hypercapnia during (top right) and a schematic drawing of the data analysis work flow by the newly developed Matlab script. **(B)** Quantification of maximal diameter changes in different vessel segments at different ages following whisker stimulation. Pial vessel reactivity increased with age (*$P < 0.05$: 6–8 weeks vs. 1 year and ***$P < 0.001$: 6–8 week vs. 2 year) while over all the capillary response was reduced in 2-year-old mice in comparison to young and 1-year-old mice. **(C)** Quantification of maximal diameter changes in different vessel segments at different ages following hypercapnia. Neurovascular reactivity of cerebral capillaries was impaired in 2-year-old mice as compared to 6–8 weeks and 1-year-old mice (*$P < 0.05$: 1 year vs. 2 year) (mean ± SEM, $n = 4$–10 mice/group, One-way ANOVA).

Reduced Vasodilation During NVC and Hypercapnia in Aged Mice

To directly visualize vascular reactivity in young, adult, and aged mice, animals received the plasma label FITC dextran and cerebral microvessels we imaged by *in vivo* 2-PM. Time series were recorded with the Zen® software (Zeiss, Oberkochen, Germany). Afterwards, original files were processed with our novel, investigator-independent vessel diameter measurement script and diameter changes of different vessel segments (pial arterioles, penetrating arterioles, and capillaries) were analyzed. A straight line crossing the investigated vessel at an angle of 90° was drawn and the inner diameter of the vessel was assessed based on the fluorescence of the injected plasma marker. Absolute changes of vessel diameter following whisker stimulation or hypercapnia were calculated by the script and expressed as % baseline (**Figure 3A**). A total of three whisker stimulations and one CO_2 challenge were performed and analyzed.

The most pronounced vasodilation was observed in capillaries independent of the age of the animals or the stimulation paradigm (**Figures 3B,C**). Two-year-old mice showed a reduced response in penetrating arterioles and in capillaries, specifically after hypercapnia (**Figure 3C**, $^{*}P < 0.05$: 1 year vs. 2 year), suggesting a spatially distinct effect of age on cerebrovascular reactivity.

DISCUSSION

In the current study, we developed two Matlab-based software tools, the "NVC-ToolBox," to analyze neurovascular reactivity by *in vivo* LSCI and 2-PM imaging following whisker stimulation and hypercapnia. The NVC-ToolBox allowed us to analyze neurovascular reactivity in a fully blinded, automatized, fast, and user-friendly manner. Moreover, we used aging as a paradigm to validate the NVC-ToolBox, since aging is well-known to reduce neurovascular reactivity. Our results demonstrate that the NVC-ToolBox is an easy to use and reliable tool for the assessment of neurovascular reactivity. Statistically significant changes in neurovascular reactivity between groups could be identified with a group size of six animals and a reasonable variability. Further, the time needed to analyze the data could be shortened by over 90% and investigator bias was completely eliminated from the analysis process. In the manual analysis procedure, first, frames of 2-PM time series must be exported as separate images which is between 250 and 280 frames. Then these images are binarized, skeletonized and diameters were measured by another plugin using ImageJ software. This procedure takes for the manual analyzer approximately 5 min for each image. However, with the automated tool it takes only 1–2 s to analyze all frames. Therefore the differences between the manual and automated analysis in sense of time and quality is massive. In terms of the effect of age on neurovascular reactivity, our data suggest a differential response during aging. Further, 2-PM imaging revealed a distinct involvement of different vessel segments following NVC and hypercapnia, i.e., the most pronounced vasodilation was found primarily at the capillary level and aging reduced vascular reactivity mainly in this vascular bed; to our surprise pial arteriole reactivity following whisker stimulation was even increased during the aging.

NVC ensures rapid CBF regulation in response to neuronal activity. *In vivo* imaging techniques with a high spatiotemporal resolution are crucial for understanding changes in NVC, a process critical in many pathologies such as aging or dementia. Moreover, reliable assessment of NVC is only possible with proper surgical window preparations, stable animal physiology, reliable and reproducible stimulation modalities, precise data acquisition, and objective image analysis algorithms (38). One of the gold standard techniques for NVC measurements is LSCI which is a simple, non-invasive *in vivo* imaging technique for the measurement of tissue perfusion (39–43). When moving objects are illuminated by dispersed laser light, the scattered light will form an interference ("speckle") pattern, which is proportional to tissue perfusion (44, 45). This technique is well-established and frequently used for dynamic imaging of CBF thanks to its high temporal resolution (11). When NVC is induced by forepaw, hind paw, or whisker stimulation, cerebral arterioles in the respective cortical area dilate to redistribute blood flow to the activated area. The subsequent increase in CBF can be visualized by 2-D heat maps using LSCI. Commercially available LSCI devices display, store and allow analyzing heat maps of individual animals, however, lack modalities to analyze data from cohorts of animals, specifically longitudinally. Since CBF responses can be spatially distinct and vary in intensity, changes often became only apparent when individual values of a group of animals are averaged or superimposed. This approach termed "co-registration" is not completely novel, since it has already been successfully used for the analysis of large cohorts of human and animal MRI, BOLD, or PET data (46, 47), however, it has, to the best of our knowledge, never been employed for the analysis of LSCI data sets. Using the NVC-ToolBox, multiple stimulations from the same subject and multiple subjects from the same experimental group can be averaged and high-resolution images displaying the mean response are created in a fully blinded and automated manner. Using this novel analysis tool, we observed that following whisker stimulation, young mice show a focal CBF response in the middle of the whisker area, while, 1-year-old mice showed a higher response covering almost the whole somatosensory cortex. In 2-year-old mice the response was focused again, but weak (**Figure 1B**). The observed changes in the spatial distribution of the laser speckle recordings could be linked to different factors. We can speculate that either the vascularization or the vascular function (or both) change with age. Many laboratories reported a reduction of capillary number and density in the aged brain (48–51). Others reported a substantial age-related decrease in brain arteriolar density in 24 vs. 13 months old rats (52–54). Some studies suggest that age-related changes can be multiphasic in the sense that capillary density increases during late adulthood and then declines at advanced ages in humans and rats (55, 56). Li et al. suggested a reduced capillary density together with a higher capillary flow velocity and heterogeneous capillary flow pattern in older vs. younger mice by using optical coherence tomography angiography (57). Therefore, oxygen delivery may be reduced during aging (58). Despite these data on vessel density and vessel

function, quite little is known about cerebrovascular plasticity during the aging process. Our data suggest that aging is also associated with significant changes in the spatial CBF response, i.e., that aging induces plastic changes of the neuronal network, which is then followed, by a consecutive vascular change. Further experiments using longitudinal imaging in individual animals may answer this important issue.

Two-photon laser scanning microscopy is a state-of-the-art technique used for observing, and measuring vascular changes *in vivo* with high spatial and temporal resolution with deep tissue penetration (59). In the current study, we used 2-PM to visualize changes of the vascular diameter of different vessel segments upon whisker stimulation or hypercapnia. After acquiring 3-D image stacks from the cerebral cortex, the diameter of vessels needed to be measured in a reliable and efficient manner, since manual analysis of 2-PM data is a tedious, time-consuming, and quite subjective process. To overcome these shortcomings, we developed scripts to measure vessel diameter changes of all vessels present in the 3D stack quickly and reliably. The scripts used for the analysis of LSCI data, as well as the analysis of 2-PM data resulted in statistically significant changes in neurovascular reactivity between groups with a group size of six animals and reasonable variability. In addition, the time needed to analyze the data could be shortened significantly and investigator bias was abolished from the analysis process.

Another advantage of the currently used experimental approach is the use of two different imaging modalities investigating two different aspects of neurovascular reactivity. Two-photon microscopy allows the assessment of vessel reactivity with high spatial and temporal resolution, however, only in a very limited area of the cortex (e.g., 200 x 200 μm), while LSCI has a limited spatial resolution and depth penetration, but is able to assess CBF responses in much larger cortical areas (e.g., 4 x 4 mm or more). Hence, using these two techniques consecutively on the same animal has complementary advantages and will allow a more in depth understanding of neurovascular reactivity in the healthy and diseased brain.

Aging has multiple effects at the systemic, molecular, and cellular level and impairs, among others, cerebrovascular reactivity (8, 26, 27). In the current study, we performed whisker stimulation in three different age groups, namely young (6–8 weeks), 1-year, and 2-year-old mice. Our LSCI analysis tool successfully produced superimposed stimulation responses from individual mice and created high-resolution mean heat maps by averaging the data from a whole group of mice. After the creation of the maps, the visual data was processed with our tool to create numerical values. Thus, we observed a trend toward more pronounced neurovascular reactivity during the first year of age and significantly lower and slower responses in 2-year-old mice. These results are similar to those published by other laboratories, e.g., Park and colleagues also found a significant reduction of NVC in 2-year-old mice (27). Moeini et al. showed no significant tissue pO_2 changes to whisker stimulation at the age of 15–16 months but a significant reduction at the age of 26–28 months (60). On the other hand Tucsek et al. (61) found a decreased NVC response at the age of 7 months by using laser doppler. Soleimanzad et al. also revealed a decreased response to odor stimulation at the age of 10 months by using multiexposure speckle imaging (36). Various results can be related to measurement techniques and response of specific cortex regions to specific stimuli can be differently affected during aging (60). Thus, the NVC-ToolBox generated data in line with the current literature.

Besides whisker response, 2-year-old mice had a reduced and slow vessel dilatation following hypercapnia, while 1-year-old mice showed no pathological response (**Figure 2B**). This data suggests that at the age of 1 year maximal dilation potential of the vessels maintain their ability to fully dilate while this function is significantly impaired by aging. Munting et al. showed no significant differences between young and 1-year-old mice to a 7.5% CO_2 challenge by arterial spin labeling (62). In the current study we recorded a ∼30% CBF increase following hypercapnia in young mice. Other studies, using different imaging techniques and anesthesia protocols, recorded values from 20 to 60% (8, 62, 63). These differences between laboratories emphasize the necessity for standardized and reproducible protocols for the assessment of neurovascular functions.

The analysis of vessel diameters at a depth of up to 100 μm within the cerebral cortex by 2-PM showed an increase in vascular reactivity toward smaller vessels, i.e., the highest response at the level of cortical capillaries. This observation was most pronounced in 1-year-old mature mice and almost eliminated in aged mice. Overall, neurovascular reactivity was reduced in 2-year-old mice in almost all vascular beds, except in pial vessels. This data suggest that different vessel segments react differently to sensory stimuli and that functional deterioration of the capillary bed might be the primary reason for reduced neurovascular reactivity and loss of vascular integrity during aging process (54). In fact, it has been reported that the tortuosity of the whole neurovascular tree (middle, anterior and posterior cerebral arterioles, penetrating arterioles, and capillaries) increases with age in mice and humans (64–67). Hence, such anatomical changes may well be part of the explanation why the functionality of the neurovascular network decreases with age. Moreover, distinct structural and functional characteristics of different vessel segments may explain why aging may have a differential effect on specific vascular beds. While pial arteries have a thick layer of smooth muscle cell lining and elastic lamina, penetrating arterioles have a thin smooth muscle layer, which gets completely lost while they dive deeper into the parenchyma. At the cerebral capillary level, endothelial cells are surrounded by a basement membrane, pericytes, and astrocytic end-feet (2, 68). Hence, these structures may be differentially affected by aging and may thus cause the observed spatially distinct neurovascular dysfunction.

Next to the degree and speed of neurovascular reactivity in different vascular beds, our data also shed some light on the signal transduction occurring along the vascular tree during NVC. A recent study from Rungta et al. showed that following neuronal stimulation blood velocity increases first in the surrounding capillary bed and only somewhat later in penetrating and pial arterioles (69), suggesting that capillaries trigger signals which are transferred to upstream arterioles and recruit them to the coupling response. Consequently, if the capillary response to

neuronal activation is disturbed, also the upstream response should be reduced or interrupted. Interestingly, we did not observe this behavior in our current experiments. On the contrary, aging reduced the reactivity of cortical capillaries, but caused a hyperactive pial response, suggesting that aging may reduce the interaction between the brain parenchyma and cerebral vessels, but that upstream signaling along the vascular tree may remain intact. Hence, reduced capillary dilatation and subsequent lack of tissue perfusion would elicit increased upstream signaling and a hyperactive pial response. Investigating the mechanisms responsible for these changes, such as paravascular nerve fibers, perivascular astrocytes, adenosine, or neuronal nitric oxide (NO) (70–72), may help to reduce age related neurovascular dysfunction. Perivascular astrocytes, for example, which connect NO producing neurons with pial arterioles, are heavily activated in the aged brain (71, 73, 74). Thus, it may be speculated that activated astrocytes trigger dilation of pial arterioles in the presence of an impaired capillary response. On the other hand, pial arterioles are richly innervated by extrinsic perivascular sympathetic and parasympathetic postganglionic neurons (20, 75). Thus, it is possible that in the aged brain loss of cholinergic innervation or noradrenergic signaling could also reveal distinct pial arteriole responses in the aged brain (54, 76). Further experiments using the current developed setup may help to answer this and similar questions in the future.

Another question is of course which cellular or molecular mechanisms are responsible for the observed impairments of neurovascular reactivity during aging. Sufficient supply of the brain parenchyma with blood depends on an intact communication between the cells in the NVU, i.e. endothelial cells, astrocytes, and pericytes. It is well-known that during aging, elements of the NVU start to deteriorate resulting in dysfunction of the blood-brain barrier and capillary dilation (77–82). Reasons for these functional impairments maybe a decline in microvascular remodeling, i.e., the missing replacement of aged cells of the neurovascular unit (83), such as pericytes (80) due to the increased production of reactive oxidative species (ROS) in the aging brain (26, 84, 85) as suggested by Fan and colleagues who found significantly increased ROS production in 2-year-old mice and human brain tissue accompanied by reduced capillary density and cognitive decline (86).

In summary, we measured the effect of aging on neurovascular reactivity using two different imaging modalities and a custom-made, investigator-independent analysis tool. We show increased neurovascular reactivity during brain maturation and reduced neurovascular reactivity during aging. Furthermore, we showed that aging does not affect all cortical vessel segments equally, but has a distinct effect on capillaries. Thus, the NVC-ToolBox turned out to be a reliable, robust, and investigator-independent tool to analyze neurovascular reactivity in the healthy and aged mouse brain.

DATA AVAILABILITY STATEMENT

The raw data supporting the conclusions of this article will be made available by the authors, without undue reservation.

ETHICS STATEMENT

The animal study was reviewed and approved by Government of Upper Bavaria (animal protocol number: Vet_2-15-196).

AUTHOR CONTRIBUTIONS

FS: manuscript preparation, data analysis, figure preparation, and supervised the findings of this work. ZF: carried out the experiments and data analysis. BG: LSCI image processing script writing. MG: 2-PM vessel analysis script writing. RS: figure preparation and proofreading. NP: designed the study, supervised the findings of this work, manuscript writing, and proofreading. All authors contributed to the article and approved the submitted version.

ACKNOWLEDGMENTS

This manuscript contains data from the MD thesis of ZF. Figures were created with BioRender.com.

REFERENCES

1. Hillman EM. Coupling mechanism and significance of the BOLD signal: a status report. *Annu Rev Neurosci.* (2014) 37:161–81. doi: 10.1146/annurev-neuro-071013-014111
2. Iadecola C. The neurovascular unit coming of age: a journey through neurovascular coupling in health and disease. *Neuron.* (2017) 96:17–42. doi: 10.1016/j.neuron.2017.07.030
3. Hu X, De Silva TM, Chen J, Faraci FM. Cerebral vascular disease and neurovascular injury in ischemic stroke. *Circ Res.* (2017) 120:449–71. doi: 10.1161/CIRCRESAHA.116.308427
4. Nicolakakis N, Hamel E. Neurovascular function in Alzheimer's disease patients and experimental models. *J Cereb Blood Flow Metab.* (2011) 31:1354–70. doi: 10.1038/jcbfm.2011.43
5. Hinzman JM, Andaluz N, Shutter LA, Okonkwo DO, Pahl C, Strong AJ, et al. Inverse neurovascular coupling to cortical spreading depolarizations in severe brain trauma. *Brain.* (2014) 137:2960–72. doi: 10.1093/brain/awu241
6. Tiret P, Chaigneau E, Lecoq J, Charpak S. Two-photon imaging of capillary blood flow in olfactory bulb glomeruli. *Methods Mol Biol (Clifton, NJ).* (2009) 489:81–91. doi: 10.1007/978-1-59745-543-5_4
7. van Veluw SJ, Hou SS, Calvo-Rodriguez M, Arbel-Ornath M, Snyder AC, Frosch MP, et al. Vasomotion as a driving force for paravascular clearance in the awake mouse brain. *Neuron.* (2020) 105:549–561.e545. doi: 10.1016/j.neuron.2019.10.033
8. Balbi M, Ghosh M, Longden TA, Jativa Vega M, Gesierich B, Hellal F, et al. Dysfunction of mouse cerebral arteries during early aging. *J Cereb Blood Flow Metab.* (2015) 35:1445–53. doi: 10.1038/jcbfm.2015.107
9. Hayashi A, Yoshida T, Ohki K. Cell type specific representation of vibro-tactile stimuli in the mouse primary somatosensory cortex. *Front Neural Circuits.* (2018) 12:109. doi: 10.3389/fncir.2018.00109
10. Wang Z, Hughes S, Dayasundara S, Menon RS. Theoretical and experimental optimization of laser speckle contrast imaging for high specificity to brain microcirculation. *J Cereb Blood Flow Metab.* (2007) 27:258–69. doi: 10.1038/sj.jcbfm.9600357

11. Dunn AK, Bolay H, Moskowitz MA, Boas DA. Dynamic imaging of cerebral blood flow using laser speckle. *J Cereb Blood Flow Metab.* (2001) 21:195–201. doi: 10.1097/00004647-200103000-00002
12. Bolay H, Reuter U, Dunn AK, Huang Z, Boas DA. Moskowitz MA. Intrinsic brain activity triggers trigeminal meningeal afferents in a migraine model. *Nat Med.* (2002) 8:136–42. doi: 10.1038/nm0202-136
13. Lind BL, Jessen SB, Lønstrup M, Joséphine C, Bonvento G, Lauritzen M. Fast Ca(2+) responses in astrocyte end-feet and neurovascular coupling in mice. *Glia.* (2018) 66:348–58. doi: 10.1002/glia.23246
14. Shih AY, Driscoll JD, Drew PJ, Nishimura N, Schaffer CB, Kleinfeld D. Two-photon microscopy as a tool to study blood flow and neurovascular coupling in the rodent brain. *J Cereb Blood Flow Metab.* (2012) 32:1277–309. doi: 10.1038/jcbfm.2011.196
15. Chow BW, Nuñez V, Kaplan L, Granger AJ, Bistrong K, Zucker HL, et al. Caveolae in CNS arterioles mediate neurovascular coupling. *Nature.* (2020) 579:106–10. doi: 10.1038/s41586-020-2026-1
16. Csipo T, Mukli P, Lipecz A, Tarantini S, Bahadli D, Abdulhussein O, et al. Assessment of age-related decline of neurovascular coupling responses by functional near-infrared spectroscopy (fNIRS) in humans. *GeroScience.* (2019) 41:495–509. doi: 10.1007/s11357-019-00122-x
17. Svennerholm L, Bostrom K. Jungbjer, B. Changes in weight and compositions of major membrane components of human brain during the span of adult human life of Swedes. *Acta Neuropathol.* (1997) 94:345–52. doi: 10.1007/s004010050717
18. Petralia RS, Mattson MP, Yao PJ. Communication breakdown: the impact of ageing on synapse structure. *Ageing Res Rev.* (2014) 14:31–42. doi: 10.1016/j.arr.2014.01.003
19. Gorelick PB, Scuteri A, Black SE, Decarli C, Greenberg SM, Iadecola C, et al. Vascular contributions to cognitive impairment and dementia: a statement for healthcare professionals from the american heart association/american stroke association. *Stroke.* (2011) 42:2672–713. doi: 10.1161/STR.0b013e3182299496
20. Phillips AA, Chan FH, Zheng MM, Krassioukov AV, Ainslie PN. Neurovascular coupling in humans: physiology, methodological advances and clinical implications. *J Cereb Blood Flow Metab.* (2016) 36:647–64. doi: 10.1177/0271678X15617954
21. Tarantini S, Csiszar A, Ungvari Z. Midlife obesity impairs neurovascular coupling responses. *Obesity (Silver Spring).* (2021) 29:17. doi: 10.1002/oby.23072
22. Cooper LL, Woodard T, Sigurdsson S, van Buchem MA, Torjesen AA, Inker LA, et al. Cerebrovascular damage mediates relations between aortic stiffness and memory. *Hypertension.* (2016) 67:176–82. doi: 10.1161/HYPERTENSIONAHA.115.06398
23. Zaletel M, Strucl M, Pretnar-Oblak J, Zvan B. Age-related changes in the relationship between visual evoked potentials and visually evoked cerebral blood flow velocity response. *Funct Neurol.* (2005) 20:115–20.
24. Topcuoglu MA, Aydin H, Saka E. Occipital cortex activation studied with simultaneous recordings of functional transcranial Doppler ultrasound (fTCD) and visual evoked potential (VEP) in cognitively normal human subjects: effect of healthy aging. *Neurosci Lett.* (2009) 452:17–22. doi: 10.1016/j.neulet.2009.01.030
25. Stefanova I, Stephan T, Becker-Bense S, Dera T, Brandt T, Dieterich M. Age-related changes of blood-oxygen-level-dependent signal dynamics during optokinetic stimulation. *Neurobiol Aging.* (2013) 34:2277–86. doi: 10.1016/j.neurobiolaging.2013.03.031
26. Toth P, Tarantini S, Tucsek Z, Ashpole NM, Sosnowska D, Gautam T, et al. Resveratrol treatment rescues neurovascular coupling in aged mice: role of improved cerebromicrovascular endothelial function and downregulation of NADPH oxidase. *Am J Physiol Heart Circ Physiol.* (2014) 306:H299–308. doi: 10.1152/ajpheart.00744.2013
27. Park L, Anrather J, Girouard H, Zhou P, Iadecola C. Nox2-derived reactive oxygen species mediate neurovascular dysregulation in the aging mouse brain. *J Cereb Blood Flow Metab.* (2007) 27:1908–918. doi: 10.1038/sj.jcbfm.9600491
28. Tarumi T, Zhang R. Cerebral blood flow in normal aging adults: cardiovascular determinants, clinical implications, and aerobic fitness. *J Neurochem.* (2018) 144:595–608. doi: 10.1111/jnc.14234
29. Ighodaro ET, Abner EL, Fardo DW, Lin AL, Katsumata Y, Schmitt FA, et al. Risk factors and global cognitive status related to brain arteriolosclerosis in elderly individuals. *J Cereb Blood Flow Metab.* (2017) 37:201–16. doi: 10.1177/0271678X15621574
30. Mayhan WG, Faraci FM, Baumbach GL, Heistad DD. Effects of aging on responses of cerebral arterioles. *Am J Physiol.* (1990) 258:H1138–43. doi: 10.1152/ajpheart.1990.258.4.H1138
31. Villeneuve S, Reed BR, Madison CM, Wirth M, Marchant NL, Kriger S, et al. Vascular risk and Abeta interact to reduce cortical thickness in AD vulnerable brain regions. *Neurology.* (2014) 83:40–7. doi: 10.1212/WNL.0000000000000550
32. de la Torre JC. Is Alzheimer's disease a neurodegenerative or a vascular disorder? Data, dogma, and dialectics. *Lancet Neurol.* (2004) 3:184–90. doi: 10.1016/S1474-4422(04)00683-0
33. Viswanathan A, Rocca WA. Tzourio, C. Vascular risk factors and dementia: how to move forward? *Neurology.* (2009) 72:368–74. doi: 10.1212/01.wnl.0000341271.90478.8e
34. Zlokovic BV. Neurovascular pathways to neurodegeneration in Alzheimer's disease and other disorders. *Nat Rev Neurosci.* (2011) 12:723–38. doi: 10.1038/nrn3114
35. Lipecz A, Csipo T, Tarantini S, Hand RA, Ngo BN, Conley S, et al. Age-related impairment of neurovascular coupling responses: a dynamic vessel analysis (DVA)-based approach to measure decreased flicker light stimulus-induced retinal arteriolar dilation in healthy older adults. *GeroScience.* (2019) 41:341–9. doi: 10.1007/s11357-019-00078-y
36. Soleimanzad H, Montaner M, Ternier G, Lemitre M, Silvestre JS, Kassis N, et al. Obesity in midlife hampers resting and sensory-evoked cerebral blood flow in mice. *Obesity (Silver Spring).* (2021) 29:150–8. doi: 10.1002/oby.23051
37. Bailey-Downs LC, Tucsek Z, Toth P, Sosnowska D, Gautam T, Sonntag WE, et al. Aging exacerbates obesity-induced oxidative stress and inflammation in perivascular adipose tissue in mice: a paracrine mechanism contributing to vascular redox dysregulation and inflammation. *J Gerontol A Biol Sci Med Sci.* (2013) 68:780–92. doi: 10.1093/gerona/gls238
38. Yoon JH, Jeong, Y. *In vivo* imaging for neurovascular disease research. *Arch Pharm Res.* (2019) 42:263–73. doi: 10.1007/s12272-019-01128-x
39. Tarantini S, Fulop GA, Kiss T, Farkas E, Zölei-Szénási D, Galvan V, et al. Demonstration of impaired neurovascular coupling responses in TG2576 mouse model of Alzheimer's disease using functional laser speckle contrast imaging. *GeroScience.* (2017) 39:465–73. doi: 10.1007/s11357-017-9980-z
40. Winship IR. Laser speckle contrast imaging to measure changes in cerebral blood flow. *Methods Mol Biol (Clifton, NJ).* (2014) 1135:223–35. doi: 10.1007/978-1-4939-0320-7_19
41. Ma J, Ma Y, Shuaib A, Winship IR. Impaired collateral flow in pial arterioles of aged rats during ischemic stroke *Transl Stroke Res.* (2020) 11:243–53. doi: 10.1007/s12975-019-00710-1
42. Xie Y, Chen S, Anenberg E, Murphy TH. Resistance of optogenetically evoked motor function to global ischemia and reperfusion in mouse in vivo. *J Cereb Blood Flow Metab.* (2013) 33:1148–52. doi: 10.1038/jcbfm.2013.89
43. Mastantuono T, Starita N, Battiloro L, Di Maro M, Chiurazzi M, Nasti G, et al. Laser speckle imaging of rat pial microvasculature during hypoperfusion-reperfusion damage. *Front Cell Neurosci 11:298.* (2017). doi: 10.3389/fncel.2017.00298
44. Kazmi SM, Richards LM, Schrandt CJ, Davis MA, Dunn AK. Expanding applications, accuracy, and interpretation of laser speckle contrast imaging of cerebral blood flow. *J Cereb Blood Flow Metab.* (2015) 35:1076–84. doi: 10.1038/jcbfm.2015.84
45. Yuan S, Devor A, Boas DA, Dunn AK. Determination of optimal exposure time for imaging of blood flow changes with laser speckle contrast imaging. *Appl Opt.* (2005) 44:1823–30. doi: 10.1364/AO.44.001823
46. Aanerud J, Borghammer P, Chakravarty MM, Vang K, Rodell AB, Jonsdottir KY, et al. Brain energy metabolism and blood flow differences in healthy aging. *J Cereb Blood Flow Metab.* (2012) 32:1177–87. doi: 10.1038/jcbfm.2012.18
47. Chao TH, Chen JH, Yen, CT. Plasticity changes in forebrain activity and functional connectivity during neuropathic pain development in rats with sciatic spared nerve injury *Mol Brain.* (2018) 11:55. doi: 10.1186/s13041-018-0398-z
48. Amenta F, Cavallotti D, Del Valle M, Mancini M, Naves FJ, Vega JA. et al. Age-related changes in brain microanatomy: sensitivity to treatment with the

dihydropyridine calcium channel blocker darodipine (PY 108-068). *Brain Res Bull.* (1995) 36:453–60. doi: 10.1016/0361-9230(94)00210-R
49. Casey MA, Feldman ML. Aging in the rat medial nucleus of the trapezoid body III Alterations in capillaries. *Neurobiol Aging.* (1985) 6:39–46. doi: 10.1016/0197-4580(85)90070-3
50. Jucker M, Bättig K, Meier-Ruge W. Effects of aging and vincamine derivatives on pericapillary microenvironment: stereological characterization of the cerebral capillary network. *Neurobiol Aging.* (1990) 11:39–46. doi: 10.1016/0197-4580(90)90060-D
51. Brown WR, Moody DM, Thore CR, Challa VR, Anstrom, J*A*. Vascular dementia in leukoaraiosis may be a consequence of capillary loss not only in the lesions, but in normal-appearing white matter and cortex as well. *J Neurol Sci.* (2007) 257:62–6. doi: 10.1016/j.jns.2007.01.015
52. Hutchins PM, Lynch CD, Cooney PT, Curseen KA. The microcirculation in experimental hypertension and aging. *Cardiovasc Res.* (1996) 32:772–80. doi: 10.1016/S0008-6363(96)00136-8
53. Sonntag WE, Lynch CD, Cooney PT, Hutchins PM. Decreases in cerebral microvasculature with age are associated with the decline in growth hormone and insulin-like growth factor 1. *Endocrinology.* (1997) 138:3515–20. doi: 10.1210/endo.138.8.5330
54. Farkas E, Luiten PG. Cerebral microvascular pathology in aging and Alzheimer's disease. *Progress Neurobiol.* (2001) 64:575–611. doi: 10.1016/S0301-0082(00)00068-X
55. Hunziker O, Abdel'Al S, Schulz U. The aging human cerebral cortex: a stereological characterization of changes in the capillary net. *J Gerontol.* (1979) 34:345–50. doi: 10.1093/geronj/34.3.345
56. Wilkinson JH, Hopewell JW, Reinhold HS. A quantitative study of age-related changes in the vascular architecture of the rat cerebral cortex. *Neuropathol Appl Neurobiol.* (1981). 7:451–62. doi: 10.1111/j.1365-2990.1981.tb00245.x
57. Li Y, Choi WJ, Wei W, Song S, Zhang Q, Liu J, et al. Aging-associated changes in cerebral vasculature and blood flow as determined by quantitative optical coherence tomography angiography. *Neurobiol Aging.* (2018) 70:148–59. doi: 10.1016/j.neurobiolaging.2018.06.017
58. Østergaard L, Jespersen SN, Engedahl T, Gutiérrez Jiménez E, Ashkanian M, Hansen MB, et al. Capillary dysfunction: its detection and causative role in dementias and stroke. *Curr Neurol Neurosci Rep.* (2015) 15:37. doi: 10.1007/s11910-015-0557-x
59. Kleinfeld D, Mitra PP, Helmchen F, Denk W. Fluctuations and stimulus-induced changes in blood flow observed in individual capillaries in layers 2 through 4 of rat neocortex. *Proc Natll Acad Sci U S A.* (1998) 95:15741–6. doi: 10.1073/pnas.95.26.15741
60. Moeini M, Lu X, Bélanger S, Picard F, Boas D, Kakkar A, et al. Cerebral tissue pO(2) response to stimulation is preserved with age in awake mice. *Neurosci Lett.* (2019) 699:160–66. doi: 10.1016/j.neulet.2019.02.007
61. Tucsek Z. TothP, Tarantini S, Sosnowska D, Gautam T, Warrington JP, et al. Aging exacerbates obesity-induced cerebromicrovascular rarefaction, neurovascular uncoupling, and cognitive decline in mice. *J Gerontol A Biol Sci Med Sci.* (2014) 69:1339–52. doi: 10.1093/gerona/glu080
62. Munting LP, Derieppe MPP, Suidgeest E, Denis de Senneville B, Wells JA, van der Weerd L. Influence of different isoflurane anesthesia protocols on murine cerebral hemodynamics measured with pseudo-continuous arterial spin labeling. *NMR Biomed.* (2019) 32:e4105. doi: 10.1002/nbm.4105
63. Wenzel J, Hansen CE, Bettoni C, Vogt MA, Lembrich B, Natsagdorj R, et al. Impaired endothelium-mediated cerebrovascular reactivity promotes anxiety and respiration disorders in mice. *Proc Natl Acad Sci U S A.* (2020) 117:1753–61. doi: 10.1073/pnas.1907467117
64. Faber JE, Zhang H, Lassance-Soares RM, Prabhakar P, Najafi AH, Burnett MS, et al. Aging causes collateral rarefaction and increased severity of ischemic injury in multiple tissues. *Arteriosclerosis Thrombosis Vasc Biol.* (2011) 31:1748–56. doi: 10.1161/ATVBAHA.111.227314
65. Kang HM, Sohn I, Jung J, Jeong JW, Park, C. Age-related changes in pial arterial structure and blood flow in mice. *Neurobiol Aging.* (2016) 37:161–70. doi: 10.1016/j.neurobiolaging.2015.09.008
66. Bullitt E, Zeng D, Mortamet B, Ghosh A, Aylward SR, Lin W, et al. The effects of healthy aging on intracerebral blood vessels visualized by magnetic resonance angiography. *Neurobiol Aging.* (2010) 31:290–300. doi: 10.1016/j.neurobiolaging.2008.03.022
67. Thore CR, Anstrom JA, Moody DM, Challa VR, Marion MC, Brown, W*R*. Morphometric analysis of arteriolar tortuosity in human cerebral white matter of preterm, young, and aged subjects. *J Neuropathol Exp Neurol.* (2007) 66:337–45. doi: 10.1097/nen.0b013e3180537147
68. Sweeney MD, Ayyadurai S, Zlokovic B*V*. Pericytes of the neurovascular unit: key functions and signaling pathways. *Nat Neurosci.* (2016) 19:771–83. doi: 10.1038/nn.4288
69. Rungta RL, Zuend M, Aydin AK, Martineau É, Boido D, Weber B, et al. Diversity of neurovascular coupling dynamics along vascular arbors in layer II/III somatosensory cortex. *Commun Biol.* (2021) 4:855. doi: 10.1038/s42003-021-02382-w
70. Petzold GC, Murthy, VN. Role of astrocytes in neurovascular coupling. *Neuron.* (2011) 71:782–97. doi: 10.1016/j.neuron.2011.08.009
71. Koehler RC, Gebremedhin D, Harder DR. Role of astrocytes in cerebrovascular regulation. *J Appl Physiol (Bethesda, Md: 1985).* (2006) 100:307–17. doi: 10.1152/japplphysiol.00938.2005
72. Xu HL, Mao L, Ye S, Paisansathan C, Vetri F, Pelligrino DA. Astrocytes are a key conduit for upstream signaling of vasodilation during cerebral cortical neuronal activation *in vivo*. *Am J Physiol Heart Circ Physiol.* (2008) 294:H622–32. doi: 10.1152/ajpheart.00530.2007
73. Wang H, Hitron IM, Iadecola C, Pickel VM. Synaptic and vascular associations of neurons containing cyclooxygenase-2 and nitric oxide synthase in rat somatosensory cortex. *Cerebr Cortex (New York, NY: 1991).* (2005) 15:1250–60. doi: 10.1093/cercor/bhi008
74. Pan J, Ma N, Yu B, Zhang W, Wan, J. Transcriptomic profiling of microglia and astrocytes throughout aging. *J Neuroinflamm.* (2020) 17:97. doi: 10.1186/s12974-020-01774-9
75. Hamel E. Perivascular nerves and the regulation of cerebrovascular tone. *J Appl Physiol (Bethesda, Md: 1985).* (2006) 100:1059–64. doi: 10.1152/japplphysiol.00954.2005
76. Lecrux C, Hamel E. Neuronal networks and mediators of cortical neurovascular coupling responses in normal and altered brain states. *Philos Trans R Soc Lond B Biol Sci.* (2016) 371:20150350. doi: 10.1098/rstb.2015.0350
77. Duncombe J, Lennen RJ, Jansen MA, Marshall I, Wardlaw JM, Horsburgh, K. Ageing causes prominent neurovascular dysfunction associated with loss of astrocytic contacts and gliosis. *Neuropathol Appl Neurobiol.* (2017) 43:477–91. doi: 10.1111/nan.12375
78. Clarke LE, Liddelow SA, Chakraborty C. MunchAE, Heiman M, Barres BA. Normal aging induces A1-like astrocyte reactivity. *Proc Natl Acad Sci U S A.* (2018) 115:E1896–905. doi: 10.1073/pnas.1800165115
79. Tarantini S, Tran CHT, Gordon GR, Ungvari Z, Csiszar A. Impaired neurovascular coupling in aging and Alzheimer's disease: contribution of astrocyte dysfunction and endothelial impairment to cognitive decline. *Exp Gerontol.* (2017) 94:52–58. doi: 10.1016/j.exger.2016.11.004
80. Bell RD, Winkler EA, Sagare AP, Singh I, LaRue B, Deane R, et al. Pericytes control key neurovascular functions and neuronal phenotype in the adult brain and during brain aging. *Neuron.* (2010) 68:409–427. doi: 10.1016/j.neuron.2010.09.043
81. Yang AC, Stevens MY, Chen MB, Lee DP, Stahli D, Gate D, et al. Physiological blood-brain transport is impaired with age by a shift in transcytosis. *Nature.* (2020) 583:425–430. doi: 10.1038/s41586-020-2453-z
82. Kiss T, Nyul-Toth A, Balasubramanian P, Tarantini S, Ahire C, DelFavero J, et al. Single-cell RNA sequencing identifies senescent cerebromicrovascular endothelial cells in the aged mouse brain. *GeroScience.* (2020) 42:429–444. doi: 10.1007/s11357-020-00177-1
83. Harb R, Whiteus C, Freitas C, Grutzendler J. *In vivo* imaging of cerebral microvascular plasticity from birth to death. *J Cereb Blood Flow Metab.* (2013) 33:146–56. doi: 10.1038/jcbfm.2012.152
84. Lourenço CF, Ledo A, Caetano M, Barbosa RM, Laranjinha J. Age-dependent impairment of neurovascular and neurometabolic coupling in the hippocampus. *Front Physiol.* (2018) 9:913. doi: 10.3389/fphys.2018.00913

85. Tarantini S, Valcarcel-Ares MN, Toth P, Yabluchanskiy A, Tucsek Z, Kiss T, et al. Nicotinamide mononucleotide (NMN) supplementation rescues cerebromicrovascular endothelial function and neurovascular coupling responses and improves cognitive function in aged mice. *Redox Biol.* (2019) 24:101192. doi: 10.1016/j.redox.2019.101192
86. Fan LM, Geng L, Cahill-Smith S, Liu F, Douglas G, McKenzie CA, et al. Nox2 contributes to age-related oxidative damage to neurons and the cerebral vasculature. *J Clin Invest.* (2019) 129:3374–86. doi: 10.1172/JCI 125173

Conflict of Interest: The authors declare that the research was conducted in the absence of any commercial or financial relationships that could be construed as a potential conflict of interest.

Publisher's Note: All claims expressed in this article are solely those of the authors and do not necessarily represent those of their affiliated organizations, or those of the publisher, the editors and the reviewers. Any product that may be evaluated in this article, or claim that may be made by its manufacturer, is not guaranteed or endorsed by the publisher.